

Compressive Source Separation: Theory and Methods for Hyperspectral Imaging

Mohammad Golbabaee *Student Member IEEE*, Simon Arberet, and Pierre Vandergheynst

Abstract—

We propose and analyze a new model for Hyperspectral Images (HSI) based on the assumption that the whole signal is composed of a linear combination of few sources, each of which has a specific spectral signature, and that the spatial abundance maps of these sources are themselves piecewise smooth and therefore efficiently encoded via typical sparse models. We derive new sampling schemes exploiting this assumption and give theoretical lower bounds on the number of measurements required to reconstruct HSI data and recover their source model parameters. This allows us to segment hyperspectral images into their source abundance maps directly from compressed measurements. We also propose efficient optimization algorithms and perform extensive experimentation on synthetic and real datasets, which reveals that our approach can be used to encode HSI with far less measurements and computational effort than traditional CS methods.

Index Terms—Compressed sensing, source separation, hyperspectral image, linear mixture model, sparsity, proximal splitting method.

I. INTRODUCTION

HYPERSPECTRAL IMAGES (HSI) are collections of hundreds of images that have been acquired simultaneously in narrow and adjacent spectral bands, typically by airborne sensors [1], [2]. HSI are produced by expensive spectrometers that sample the light reflected from a two-dimensional area. An HSI data set is thus a “cube” with two spatial and one spectral dimensions. Hyperspectral imagery has many applications including environmental monitoring, agriculture planning or mineral exploration. The diversity of channels in HSI makes it possible to discriminate among the various materials that make up a geographical area: each of them is represented by a unique spectral signature. Accordingly, HSI are often processed via clustering or source separation methods to obtain segmentation maps locating and labeling the various materials appearing in the image. Unfortunately, having multiple channels comes at a price: the sheer volume of data makes acquisition, transmission, storage and analysis of HSI computationally very challenging. Therefore, the problem addressed in this paper is to reduce the complexity of manipulating HSI via a suitable compression or dimensionality reduction technique.

In this context the emerging *Compressive sensing* (CS) theory, which addresses the problem of recovering signals from few linear measurements, seems ideally suited [3], [4].

The authors are with the Signal Processing Laboratory LTS2, Electrical Engineering Department, École Polytechnique Fédérale de Lausanne (EPFL), Station 11, CH-1015 Lausanne, Switzerland. This work was supported in part by the EU FET program through projects SMALL (FET-225913) and UNLocX (FET-255931), and the Swiss National Science Foundation under grant 200021-117884.

E-mail: {mohammad.golbabaee, simon.arberet, pierre.vandergheynst}@epfl.ch.

The main assumption underlying CS is that the signal is sparse or compressible when expressed in a convenient basis. A signal $x \in \mathbb{R}^n$ is called k -sparse, if it is a linear combination of only $k \ll n$ vectors of a basis Ψ , and is called *compressible* if the coefficient’s magnitudes, when sorted, have a fast power-law decay. The recent literature abounds with examples of sparse models for signals and images, see for instance [5], [6].

While the CS community has mostly focused on 1D or 2D signals, not much works have been done on higher dimensional signals, in particular multi-array signals such as HSI. Extensions of wavelets basis for 3D data have been proposed [7] and rather generic sparse models have been exploited in [8], [9] for designing innovative compressive hyperspectral imagers. However, multi-array signals such as HSI have usually some structures that go beyond the sparsity assumption. Indeed, HSI can be interpreted as a mixture of sources, each of them having a specific spectral signature. This model is widely used for unmixing HSI [10]–[14], that is extracting, from the HSI, each source and their respective spectral signatures.

The main focus of this paper is to exploit, beyond the sparsity assumption, an additional structured model, the *linear mixture* model, so as to reconstruct and separate the sources of multi-array signals assuming we know their spectra (or mixing parameters) as side information. Note that this hypothesis is validated in many applications where the elements or materials composing the data are known and their spectra tabulated. This idea was first introduced in two of our conference papers [15], [16]. In this paper, we introduce and analyze a new sampling scheme, which exploits this structured model, and that has the following important properties:

- the number of measurements, or samples, does not scale with the number of channels,
- the recovery results do not depend on the conditioning of the mixing matrix (as long as the mixing spectra are linearly independent).

We propose new algorithms for HSI *compressive source separation* (CSS), that is source separation and data reconstruction from compressed measurements, which are based on exploiting the linear mixture structure and Total Variation (TV), ℓ_1 or ℓ_0 regularization [17]–[20]. We establish that sources can be efficiently separated directly on the compressed measurements, i.e avoiding to run a source separation algorithm on this high-dimensional raw data, thereby eliminating this important bottleneck and providing a rather striking example of compressed domain data processing. We provide theoretical guaranties and intensive experiments which show that, with this approach, we can reconstruct a multi-array signal from compressed measurements with a far better accuracy than traditional CS approaches. For example, we are able to reconstruct HSI

datasets with only 3% relative error from 3% of measurements and less than 0.1% of data transmission, with an algorithm that is about 30 times faster than the conventional recovery methods. While the main target application of this paper is HSI, our model and the theoretical analysis is general and could be applied to other multi-array signals like e.g. Positive Emission Tomography (PET) or distributed sensing.

The remainder of this paper is structured as follows. The necessary background and notations are first introduced in Section II. We then propose, in Section III, two acquisition schemes that exploit the prior knowledge of the mixing parameters so as to perform a decorrelation step. In Section IV, we provide theoretical guarantees for both source identification and data reconstruction. We determine the number of CS measurements sufficient for robust source identification and signal reconstruction as a function of the sparsity of the sources, sampling SNR and the conditioning of their corresponding mixture parameters. In Section V we discuss in further details the application of our acquisition and recovery schemes for HSI. We introduce different recovery algorithms that we compare with the classical methods, for various CS acquisition schemes on two sets of HSI. Finally, in the spirit of reproducible research, the code and data needed to reproduce the experimental sections of this paper is openly available at http://unlocbox.sourceforge.net/rr/image_source_separation/.

II. BACKGROUND AND NOTATIONS

A. CS of Multichannel Signals

We represent a multichannel signal with a matrix $X \in \mathbb{R}^{n_1 \times n_2}$ where n_2 is the number of channels and n_1 is the dimension of signal in each channel. The CS acquisition protocol of a multichannel signal X is a linear mapping $\mathcal{A} : \mathbb{R}^{n_1 \times n_2} \rightarrow \mathbb{R}^m$ of X into a CS measurement vector $y \in \mathbb{R}^m$ contaminated by the measurement noise $z \in \mathbb{R}^m$:

$$y = \mathcal{A}(X) + z. \quad (1)$$

When $m \ll n_1 n_2$ the signal is effectively compressed. The main goal of CS is to recover the signal X from the fewest amount of measurements m . Note that any linear mapping $\mathcal{A}(X)$ can be written in matrix form $AX_{vec} := \mathcal{A}(X)$, where $A \in \mathbb{R}^{m \times n_1 n_2}$ and $X_{vec} \in \mathbb{R}^{n_1 n_2}$ is the vectorized form of matrix $X \in \mathbb{R}^{n_1 \times n_2}$:

$$y = AX_{vec} + z. \quad (2)$$

Recovering the sparsest X_{vec} which is consistent with the measurement error, amounts to the ℓ_0 -minimization problem:

$$\arg \min_{X_{vec}} \|X_{vec}\|_{\ell_0} \quad s.t. \quad \|y - AX_{vec}\|_2 \leq \varepsilon, \quad (3)$$

where ε is an upper bound on the norm of the noise vector (i.e. $\|z\|_2 \leq \varepsilon$), $\|\cdot\|_{\ell_0}$ denotes the ℓ_0 quasi-norm of a vector (i.e., the number of its nonzero coefficients). Unfortunately, this combinatorial minimization problem is NP-hard in general [21]. However, there are two tractable alternatives to solve problem (3): The convex relaxation leading to ℓ_1 -minimization [18], [19], and greedy algorithms such as Matching Pursuits (MP) [22] or Iterative Hard Thresholding (IHT) [20]. Both approaches provide guarantees, depending on A and the sparsity

k , so that their solutions coincide with the original signal X_{vec} , and thus with the solution of (3).

The ℓ_1 minimization approach consists in solving the following non-smooth convex optimization problem called Basis Pursuit DeNoising (BPDN):

$$\arg \min_{X_{vec}} \|X_{vec}\|_1 \quad s.t. \quad \|y - AX_{vec}\|_2 \leq \varepsilon, \quad (4)$$

where $\|\cdot\|_1$ denotes the ℓ_1 norm, which is equal to the sum of the absolute values of the vector entries, $\|\cdot\|_2$ denotes the ℓ_2 or Euclidean norm. It has been shown in [3], [4], [23] that approximating the sparse recovery problem by the ℓ_1 minimization (4) can stably recover the $K = kn_2$ sparse original solution (i.e. k -sparse signal per channel) whenever A satisfies the following property:

Definition 1. A matrix A satisfies the restricted isometry property (RIP), if for all K -sparse vectors X_{vec} , there exists a constant $\delta_K(A) \leq \sqrt{2} - 1$ for which the following inequalities hold:

$$\left(1 - \delta_K(A)\right) \|X_{vec}\|_2^2 \leq \|AX_{vec}\|_2^2 \leq \left(1 + \delta_K(A)\right) \|X_{vec}\|_2^2 \quad (5)$$

This result guarantees that sparse signals can be perfectly recovered from noise-free measurements and the recovery process is robust to noise. The computation of the isometry constants for a given matrix is prohibitive in practice, but certain classes of matrices, such as matrices with independent Gaussian or Bernoulli entries, obey the RIP condition with high probability (see Theorem 5.2 in [24]) as long as:

$$m \geq c n_2 k \log(n_1/k). \quad (6)$$

for a fixed constant c .

B. Sparse Regularization of a Multichannel Signal

Usually the data X_{vec} is not directly sparse, but sparse in a basis $\Psi \in \mathbb{R}^{n_1 n_2 \times n_1 n_2}$. In that case, the ℓ_1 regularization approach consists in solving the following problem which generalizes problem (4):

$$\arg \min_{\Theta_{vec}} \|\Theta_{vec}\|_1 \quad s.t. \quad \|y - A\Psi\Theta_{vec}\|_2 \leq \varepsilon, \quad (7)$$

with $X_{vec} = \Psi\Theta_{vec}$. Stable reconstruction by solving problem (7) is guaranteed as long as the $A\Psi$ matrix satisfies the RIP. When the data is a multichannel image, a classical basis is a block diagonal orthonormal basis $\Psi = \text{Id}_{n_2} \otimes \Psi_{2D}$ ¹ where $\Psi_{2D} \in \mathbb{R}^{n_1 \times n_1}$ denotes a proper 2-dimensional wavelet basis.

Another classical approach to regularize the data (especially images) is the total variation (TV) penalty [17], which tends to generate images with piecewise smooth regions and sharp boundaries. Replacing the ℓ_1 norm with the TV norm on each channel X_j of the multichannel in problem (7) leads to the Total Variation De-Noising (TVDN) problem:

$$\arg \min_X \sum_{j=1}^{n_2} \|X_j\|_{TV} \quad s.t. \quad \|y - AX_{vec}\|_2 \leq \varepsilon. \quad (8)$$

¹ Id_{n_2} is the $n_2 \times n_2$ identity matrix and \otimes denotes the matrix Kronecker product.

C. The Linear Mixture Model

In a wide range of multichannel signal applications (including HSI [1]), the data matrix X is derived or can be approximated by a *sparse linear mixture* model as follows:

$$X = \mathbf{S}\mathbf{H}^T. \quad (9)$$

Here, $\mathbf{S} \in \mathbb{R}^{n_1 \times \rho}$ denotes the *source matrix* whose i th column contains the proportion of the source i at each pixel. Each source is mixed with the corresponding column of the *mixing matrix* $\mathbf{H} \in \mathbb{R}^{n_2 \times \rho}$ in order to generate the full multichannel data. Each column of \mathbf{H} contains the spectrum of the corresponding source. The observed signal in any channel $j \in \{1, \dots, n_2\}$ is thus a linear combination of ρ source signals: $X_j = \sum_{i=1}^{\rho} [\mathbf{H}]_{j,i} \mathbf{S}_i$.

D. Mixing Parameters as Side Information for Multichannel CS Recovery

In certain multichannel signal acquisition setups the mixing parameters \mathbf{H} are known at both decoder and encoder sides. In particular, this is the case in many remote sensing applications where the spectra of common materials are tabulated. Such prior efficiently restricts the degrees of freedom of the entire data matrix to the sparse coefficients of the underlying sources. Indeed, we will show that, when we know the mixing parameters \mathbf{H} , the inverse problem consisting in recovering the multichannel signal X from the measurements y in (2) is equivalent to the problem of recovering the sources \mathbf{S}_{vec} from the following measurements:

$$y = A\Phi\mathbf{S}_{vec} + z, \quad (10)$$

with $\Phi = \mathbf{H} \otimes \text{Id}_{n_1}$. The source coefficients can then be recovered by solving a convex optimization problem such as (7), where A is replaced by $A\Phi$ and the multichannel signal can be reconstructed by applying the mixing matrix to the recovered source matrix according to the linear mixture model (9). This approach has the advantage of solving two problems: i) source separation directly from the compressive measurements, ii) data compressive sampling via source separation or, equivalently, via a particular structured sparse model.

III. COMPRESSIVE MULTICHANNEL SIGNAL ACQUISITION SCHEMES

If the multichannel signal follows the linear mixture model (9), the knowledge of the mixing matrix can be used efficiently. The sparse source coefficients can be directly recovered from the measurements. In this section we introduce a decorrelation mechanism, applied at the acquisition process or as a post-processing step, which has two main advantages: first it leads to strong dimensionality reduction and second it improves the conditioning of the recovery problem.

A. Multichannel Recovery via Source Recovery

When we know the mixing matrix \mathbf{H} , and thanks to the property $((BCD)_{vec} = (D^T \otimes B)C_{vec})$ of the Kronecker

product, the sampling equation (2) (in the noise free case) can be written as:

$$AX_{vec} = A(\mathbf{S}\mathbf{H}^T)_{vec} = A \underbrace{(\mathbf{H} \otimes \text{Id}_{n_1})}_{\triangleq \Phi} \mathbf{S}_{vec} = A\Phi\mathbf{S}_{vec}. \quad (11)$$

Then, the ℓ_1 regularization approach for the recovery of the whole data consists in finding the sparsest coefficients vector $\Theta_{vec} \in \mathbb{R}^{\rho n_1}$ of the sources vector $\mathbf{S}_{vec} = \Psi\Theta_{vec}$ in a basis $\Psi \in \mathbb{R}^{\rho n_1 \times \rho n_1}$, where e.g. $\Psi = \text{Id}_{\rho} \otimes \Psi_{2D}$ is a block diagonal orthonormal basis, through the following minimization:

$$\arg \min_{\Theta_{vec}} \|\Theta_{vec}\|_1 \quad s.t. \quad \|y - A\Phi\Psi\Theta_{vec}\|_2 \leq \varepsilon. \quad (12)$$

This corresponds to a ‘‘synthesis’’ formulation of BPDN using a basis Ψ . The ‘‘analysis’’ formulation, which is equivalent to the synthesis one when Ψ is a basis but different when Ψ is a redundant dictionary, consists in solving the following problem with respect to the sources instead of its coefficients:

$$\arg \min_{\mathbf{S}_{vec}} \|\Psi^*\mathbf{S}_{vec}\|_1 \quad s.t. \quad \|y - A\Phi\mathbf{S}_{vec}\|_2 \leq \varepsilon, \quad (13)$$

where Ψ^* is the adjoint of the operator Ψ .

The data X can then be recovered via the mixture model $\hat{X} = \hat{\mathbf{S}}\mathbf{H}^T$, with $\hat{\mathbf{S}}_{vec}$ being either the solution of the analysis problem (13) or $\hat{\mathbf{S}}_{vec}$ being equal to $\hat{\mathbf{S}}_{vec} = \Psi\hat{\Theta}_{vec}$ with $\hat{\Theta}_{vec}$, solution of the synthesis problem (12).

B. Decorrelation Scheme

We have seen in section II-A, that the conditions to recover the signal from the noisy measurements $y = AX_{vec} + z$ depend on properties (such as RIP) of the sensing matrix A . We introduce a particular structure for the sampling matrix A which benefits from the available knowledge of the mixture parameters \mathbf{H} and incorporates data decorrelation into the compressive acquisition.

1) *Decorrelating Multichannel CS Acquisition*: The decorrelation mechanism consists of applying the Moore-Penrose pseudo inverse matrix $\mathbf{H}^\dagger = (\mathbf{H}^T\mathbf{H})^{-1}\mathbf{H}^T$ [25] in order to remove the underlying dependencies among CS measurements. We therefore propose the following sampling matrix:

$$A = \mathbf{H}^\dagger \otimes \tilde{A}, \quad (14)$$

where the main sampling matrix is generated from a smaller-size $\hat{m} \times n_1$ *core sampling matrix* \tilde{A} . Note that CS imposes $\hat{m} \ll n_1$. The total number of measurements is $m = \rho\hat{m}$. Applying the sampling matrix A of (14) on multichannel data results in the following CS measurements:

$$\begin{aligned} y &= A\Phi\mathbf{S}_{vec} + z = \underbrace{(\mathbf{H}^\dagger \otimes \tilde{A})}_A \underbrace{(\mathbf{H} \otimes \text{Id}_{n_1})}_\Phi \mathbf{S}_{vec} + z, \quad (15) \\ &= \underbrace{(\text{Id}_\rho \otimes \tilde{A})}_{\triangleq \tilde{A}_\rho} \mathbf{S}_{vec} + z. \quad (16) \end{aligned}$$

The third equality comes from the following property: $(B \otimes C)(D \otimes F) = BD \otimes CF$, and \tilde{A}_ρ is a block diagonal matrix whose ρ diagonal blocks are populated with \tilde{A} : $\tilde{A}_\rho \triangleq \text{Id}_\rho \otimes \tilde{A}$.

As we can observe in (16) and thanks to the specific structure of the sampling matrix, the mixing parameters \mathbf{H} are discarded from the formulation and each source (each column of \mathbf{S}) is directly subsampled by the same matrix \tilde{A} .

2) *Uniform Multichannel CS Acquisition*: In many practical setups the acquisition scheme can not be arbitrarily chosen and is rather determined by various constraints posed by the physics of the signals and the implementation technology. Certain acquisition systems such as Rice's single-pixel hyperspectral imager [8] are using a universal random matrix to sample independently data in each channel. In this case, acquisition models such as (14), which require inter-channel interactions for compressed sampling, simply cannot be implemented. Here, the sampling matrix A in (2) is block diagonal with n_2 blocks (each applies on a certain channel) that are populated by a unique $\hat{m} \times n_1$ matrix (similarly as \tilde{A} in (16)):

$$A = \tilde{A}_{n_2} \triangleq \text{Id}_{n_2} \otimes \tilde{A}. \quad (17)$$

The total number of measurements is then $m = n_2 \hat{m}$. Reshaping y and z correspondingly into $\hat{m} \times n_2$ matrices Y (the measurement matrix) and Z (the noise matrix) leads to the following equivalent formulation:

$$Y = \tilde{A}X + Z. \quad (18)$$

3) *Decorrelation-based Uniform Sampling*: A decorrelation step similar to the one introduced in Section III-B1 can be applied on the CS measurements. It consists in multiplying the rows of the measurement matrix by $(\mathbf{H}^\dagger)^T$ and reducing the dimensionality of Y to an $\hat{m} \times \rho$ matrix as follows:

$$Y^* = Y(\mathbf{H}^\dagger)^T = \tilde{A}\mathbf{S} + Z^*, \quad (19)$$

where, $Z^* = Z(\mathbf{H}^\dagger)^T$. By reshaping Y^* and Z^* into the vectors y^* and z^* , one observes that the outcome of such *decorrelation-based uniform sampling* leads to an expression similar to (16):

$$y^* = \tilde{A}_\rho \mathbf{S}_{vec} + z^*. \quad (20)$$

This decorrelating scheme favorably reduces the dimension of the data: at the acquisition stage, the total number of samples is $n_2 \hat{m}$ but at the transmission and decoding stages the number of samples is only $\rho \hat{m} \ll n_2 \hat{m}$.

For the *decorrelating* sampling schemes described in section III-B1 and III-B3, the ℓ_1 minimization (e.g. the "synthesis" problem (12)) of section III-A takes the following form:

$$\arg \min_{\Theta_{vec}} \|\Theta_{vec}\|_1 \quad s.t. \quad \|y - \tilde{A}_\rho \Psi \Theta_{vec}\|_2 \leq \varepsilon, \quad (21)$$

which, in the noiseless case can be decoupled into ρ independent ℓ_1 minimizations, each of them corresponding to a certain source compressed by a universal matrix \tilde{A} . In Section IV we provide the theoretical analysis of such recovery scheme for various acquisition schemes.

IV. MAIN THEORETICAL ANALYSIS

Compressive sparse source recovery is closely related to the problem of compressed sensing with *redundant dictionaries* [26], [27]. Indeed, the later problem has the same formulation

as in (12) by replacing Φ by an overcomplete dictionary matrix. The first part of this section provides an overview of the CS literature on redundant dictionaries. In the second part, we derive new performance bounds that extend the former results for a larger class of dictionaries. In the third part, we cast the sparse source separation problem as a particular case of CS recovery using redundant dictionaries and we give a bound on the performance of the ℓ_1 minimization for each of the considered CS acquisition schemes (dense, uniform and decorrelated).

A. Compressed Sensing and Redundant Dictionaries

Let $x \in \mathbb{R}^n$ be a vector that is sparse in a dictionary $\mathbf{D} \in \mathbb{R}^{n \times d}$ (i.e., $x = \mathbf{D}\theta$ with, $\theta \in \mathbb{R}^d$). The ℓ_1 minimization approach for recovering θ (equivalently x) from the compressive measurements $y = Ax + z$ consists in solving:

$$\arg \min_{\theta} \|\theta\|_1 \quad s.t. \quad \|y - \mathbf{A}\mathbf{D}\theta\|_2 \leq \varepsilon, \quad (22)$$

where, $\|z\|_2 \leq \varepsilon$. Note that in this section A is a sampling matrix of size $m \times n$ and the dictionary \mathbf{D} typically contains a large number of columns ($d \gg n$).

Following [3], [4], if $\mathbf{A}\mathbf{D}$ satisfies RIP (see Definition 1) with a constant of order k , $\delta_k(\mathbf{A}\mathbf{D}) \leq \sqrt{2}-1$, then the solution $\hat{\theta}$ to (22) satisfies the following error bound:

$$\|\theta - \hat{\theta}\|_2 \leq c_0 k^{-1/2} \|\theta - \theta_k\|_1 + c_1 \varepsilon, \quad (23)$$

for some positive constants c_0, c_1 , and where θ_k is the best k -sparse approximation of θ .

Now the question is how many CS measurements are sufficient so that $\mathbf{A}\mathbf{D}$ satisfies the RIP? It has been shown in [26] that, for a certain class of random sampling matrices A (e.g., with i.i.d. Gaussian, Bernoulli or subgaussian elements), with very high probability the RIP constant $\delta_k(\mathbf{A}\mathbf{D})$ is bounded by:

$$\delta_k(\mathbf{A}\mathbf{D}) \leq \delta_k(A) + \delta_k(\mathbf{D}) + \delta_k(A)\delta_k(\mathbf{D}). \quad (24)$$

If \mathbf{D} is an orthonormal basis, then $\delta_k(\mathbf{D}) = 0$ and $\mathbf{A}\mathbf{D}$ becomes another subgaussian matrix with a similar distribution as for A and thus (24) holds with equality i.e., $\delta_k(\mathbf{A}\mathbf{D}) = \delta_k(A)$.

Considering the recovery condition using ℓ_1 minimization (i.e., $\delta_k(\mathbf{A}\mathbf{D}) \leq \sqrt{2}-1$) and the bound in (24), we can conclude that A must satisfy RIP with the following constant:

$$\delta_k(A) \leq \frac{\sqrt{2}-1-\delta_k(\mathbf{D})}{1+\delta_k(\mathbf{D})}. \quad (25)$$

Moreover, using the Johnson-Lindenstrauss lemma, it has been shown that (see Theorem 5.2 in [24]) a random matrix A whose elements are drawn independently at random from Gaussian, Bernoulli or subgaussian distributions satisfies RIP as long as we have:

$$m \geq ck \log(n/k), \quad (26)$$

for a constant c depending on the RIP constant of A i.e., the higher $\delta_k(A)$, the smaller c . If \mathbf{D} is not a unitary matrix, $\delta_k(\mathbf{D})$ becomes a positive constant and the more coherent the columns of \mathbf{D} , the larger its RIP constant. Therefore, there is a

tradeoff for compressed sensing using redundant dictionaries: redundancy can result in a more compact representations of the signals *i.e.*, smaller k , and thus less measurements are required for CS recovery using (22). Meanwhile, too much redundancy can lead to an awfully large constant in (26) implying that more CS measurements are required to overcome the uncertainties brought by over completeness.

B. Performance Bounds for Compressed Sensing using Asymmetric-RIP Dictionaries

In Section IV-C we will show that applying the classical RIP based analysis results in conditions that are too restrictive to guaranty the source recovery. Therefore in this part and in order to overcome such limitations, we derive a new theoretical performance bound that uses different notions of RIP. We begin by introducing the notions of the *asymmetric restricted isometry property* (A-RIP) and the *restricted condition number* of a dictionary \mathbf{D} .

Definition 2. For a positive integer $k \in \mathbb{N}$, an $n \times d$ matrix \mathbf{D} satisfies the *asymmetric restricted isometry property*, if for all k -sparse $x \in \mathbb{R}^d$ the following inequalities hold:

$$\mathcal{L}_k(\mathbf{D})\|x\|_2 \leq \|\mathbf{D}x\|_2 \leq \mathcal{U}_k(\mathbf{D})\|x\|_2, \quad (27)$$

where, $\mathcal{L}_k(\mathbf{D})$ and $\mathcal{U}_k(\mathbf{D})$ are correspondingly the largest and the smallest constants for which the inequalities above hold. The *restricted condition number* of \mathbf{D} is defined as:

$$\xi_k(\mathbf{D}) \triangleq \frac{\mathcal{U}_k(\mathbf{D})}{\mathcal{L}_k(\mathbf{D})}. \quad (28)$$

In addition, we use a different notion of RIP for the compression matrix A , namely, the *Dictionary Restricted Isometry Property* (D-RIP), proposed by Candes *et al.* in [27]:

Definition 3. For a positive integer $k \in \mathbb{N}$, a matrix A satisfies the *D-RIP adapted to a dictionary \mathbf{D}* as long as for all k -sparse vectors x the following inequalities hold:

$$(1 - \delta_k^*)\|\mathbf{D}x\|_2^2 \leq \|\mathbf{A}\mathbf{D}x\|_2^2 \leq (1 + \delta_k^*)\|\mathbf{D}x\|_2^2. \quad (29)$$

The *D-RIP constant* δ_k^* is the smallest constant for which the property above holds.

This definition extends the classical RIP (which deals with signals that are sparse in the canonical basis) to linear mappings that are able to stably embed all low dimensional subspaces spanned by every k columns of a redundant dictionary \mathbf{D} .

As in [27], we suppose that A is an $m \times n$ matrix drawn at random from certain distributions that satisfy the following concentration bound for any vector x :

$$\Pr \left(\left| \|Ax\|_2^2 - \|x\|_2^2 \right| > t\|x\|_2^2 \right) \leq C \exp(-cm), \quad (30)$$

for some constants C and $c > 0$ that are only depending on t . Then, A will satisfy the D-RIP for any $n \times d$ dictionary \mathbf{D} with overwhelming probability if

$$m \gtrsim \mathcal{O}(k \log(d/k)). \quad (31)$$

Remark 1. Matrices $A \in \mathbb{R}^{m \times n}$ whose elements are independently drawn at random from Gaussian, Bernoulli or (in

general) subgaussian distributions satisfy the concentration bound in (30) and therefore satisfy D-RIP for any $n \times d$ dictionary as long as $m \gtrsim \mathcal{O}(k \log(d/k))$.

Based on these definitions we establish the following theorem in order to bound the performance of the ℓ_1 minimization in (22):

Theorem 1. Given a matrix A that satisfies the D-RIP adapted to a dictionary \mathbf{D} , with the constant $\delta_{\gamma k}^* < 1/3$ where $\gamma \geq 1 + 2\xi_{\gamma k}^2(\mathbf{D})$, then the solution $\hat{\theta}$ to (22) obeys the following bound:

$$\|\theta - \hat{\theta}\|_2 \leq c'_0 k^{-1/2} \|\theta - \theta_k\|_1 + c'_1 \varepsilon, \quad (32)$$

for some positive constants c'_0, c'_1 .²

Using Remark 1, the following result is straightforward:

Corollary 1. For A whose elements are drawn independently at random from Gaussian, Bernoulli or subgaussian distributions, the solution to (22) obeys the error bound (32) with an overwhelming probability and for any dictionary with a finite Restricted Condition Number $\xi_{\gamma k}(\mathbf{D})$, if

$$m \gtrsim \gamma k \log(d/\gamma k). \quad (33)$$

Comparing to the bound (26) based on the classical RIP analysis, we see that (33) features the same scaling-order for the number of measurements. In addition, for both types of analysis the constant factors grow as the atoms of the dictionary become more coherent and therefore, more CS measurement are required.

Note that this result requires neither $\mathbf{A}\mathbf{D}$ nor the dictionary \mathbf{D} to satisfy the *classical* RIP. In the next section, we apply these results to guaranty the performance of the ℓ_1 minimization approach (12) for source identification and in particular, for the case where \mathbf{H} is not well-conditioned.

C. Theoretical Guaranties for Source Recovery using ℓ_1 Minimization

Sparse source recovery from compressive measurements using ℓ_1 minimization (12) is a particular case of the compressed sensing problem using dictionaries (22). Indeed, for the source recovery problem, θ and the dictionary matrix \mathbf{D} are replaced respectively with Θ_{vec} and $\Phi' \triangleq \Phi\Psi = (\mathbf{H} \otimes \text{Id}_{n_1})\Psi$, and consequently, $n = n_1 n_2$ and $d = \rho n_1$. The only difference here is that Φ' is a tall matrix (*i.e.*, $d \leq n$) due to its specific construction and the assumption of having few number of sources (*i.e.*, $\rho \leq n_2$). Though there is no redundancy in Φ' in terms of the number of columns, there is uncertainty at the sparse decoder because of *coherent* columns. The following lemma which has been proven in [7] (see Lemma 2 in [7]) shows that the conditioning of Φ' is directly related to the conditioning of the underlying mixture parameters *i.e.*, intuitively, if the columns of \mathbf{H} become coherent, so become the columns of Φ' .

²Proof of this theorem is available online in the Appendix of our technical report <http://infoscience.epfl.ch/record/187384>.

Lemma 1. For matrices V_1, V_2, \dots, V_ℓ with restricted isometry constants $\delta_k(V_1), \delta_k(V_2), \dots, \delta_k(V_\ell)$ respectively, we have:

$$\delta_k(V_1 \otimes V_2 \otimes \dots \otimes V_\ell) \leq \prod_{i=1}^{\ell} \left(1 + \delta_k(V_i)\right) - 1. \quad (34)$$

Since the RIP constant of any orthonormal basis is zero (e.g., $\delta_k(\text{Id}_{n_1}) = 0$), and since Ψ is an orthogonal matrix, we can deduce the following bound on the RIP constant of $\Phi' = (\mathbf{H} \otimes \text{Id}_{n_1})\Psi$ by applying Lemma 1:

$$\begin{aligned} \delta_k(\Phi') &= \delta_k(\Phi) \\ &\leq \delta_k(\mathbf{H}) \end{aligned} \quad (35)$$

$$\leq \eta \triangleq \max\left(1 - \sigma_{\min}^2(\mathbf{H}), \sigma_{\max}^2(\mathbf{H}) - 1\right). \quad (36)$$

For $k \leq \rho$ one can use (35) (which then holds with equality), and more generally (36) for any k . Note that (36) follows by the definition of the RIP constant and it only holds if \mathbf{H} is properly normalized so that $1 \leq \sigma_{\max}(\mathbf{H}) < 2$ and $0 < \sigma_{\min}(\mathbf{H}) \leq 1$.³

Moreover, due to the properties of the extreme singular values of the Kronecker product of two matrices:

$$\sigma_{\max}(V_1 \otimes V_2) = \sigma_{\max}(V_1) \sigma_{\max}(V_2), \quad (37)$$

$$\sigma_{\min}(V_1 \otimes V_2) = \sigma_{\min}(V_1) \sigma_{\min}(V_2), \quad (38)$$

and according to Definition 2, we can bound the restricted condition number of Φ' as follows:

$$\xi_k(\Phi') \leq \frac{\sigma_{\max}(\Phi')}{\sigma_{\min}(\Phi')} = \frac{\sigma_{\max}(\mathbf{H})}{\sigma_{\min}(\mathbf{H})} \triangleq \xi(\mathbf{H}), \quad (39)$$

where, $\xi(\cdot)$ (without subscript) denotes the standard definition of the condition number of a matrix. With those descriptions, the performance of the sparse source recovery using (12) can be easily characterized by any of the previous types of performance bound of sections IV-A and IV-B.

According to the standard definition of the RIP for the matrix Φ' , we can bound its restricted condition number $\xi_k(\Phi')$ as follows:

$$\xi_k(\Phi') \leq \sqrt{\frac{1 + \delta_k(\Phi')}{1 - \delta_k(\Phi')}}. \quad (40)$$

Recall that, the classical RIP based analysis in section IV-A requires $\delta_k(\Phi') < \sqrt{2} - 1$ (in order to have $\delta_k(A) > 0$ in (25)), which implies $\xi_k(\Phi') < \sqrt{\sqrt{2} + 1}$, or consequently $\xi(\mathbf{H}) < \sqrt{\sqrt{2} + 1}$. This severely restricts the application of such analysis to a limited class of relatively well-conditioned mixture parameters.

To address this limitation, we use the second theoretical analysis based on the D-RIP of the compression matrix presented in section IV-B. The following theorem is a corollary of Theorem 1:

Theorem 2. Given a mixture matrix \mathbf{H} whose condition number is $\xi(\mathbf{H})$, and a matrix A that satisfies the D-RIP adapted to $\mathbf{H} \otimes \text{Id}_{n_1}$ with the constant $\delta_{\gamma'k}^* < 1/3$ where

³This can be done by dividing \mathbf{H} and multiplying \mathbf{S} by $(\sigma_{\max}(\mathbf{H}) + \sigma_{\min}(\mathbf{H}))/2$, respectively.

$\gamma' = 1 + 2\xi^2(\mathbf{H})$, then the solution $\hat{\Theta}_{vec}$ to (12) obeys the following bound for the same constants c'_0, c'_1 as in (32):

$$\|\Theta_{vec} - \hat{\Theta}_{vec}\|_2 \leq c'_0 k^{-1/2} \|\Theta_{vec} - (\Theta_{vec})_k\|_1 + c'_1 \varepsilon. \quad (41)$$

Comparing to Theorem 1, \mathbf{D} is replaced by Φ' and γ is set to γ' which satisfies the requirement of Theorem 1 i.e., according to (39) we have $\gamma' \geq 1 + 2\xi_{\gamma'k}^2(\mathbf{H})$. As we can see, this analysis is valid for a much wider range of condition number namely, $\xi(\mathbf{H}) \leq \sqrt{\frac{n_1 n_2 / k - 1}{2}}$.⁴

Now, if we use this approximation to recover the multi-channel data i.e., $\hat{X} = \hat{\mathbf{S}}\mathbf{H}^T$, the reconstruction error can be bounded using (41) and the following inequality:

$$\begin{aligned} \|X - \hat{X}\|_F &\leq \sigma_{\max}(\mathbf{H}) \|\mathbf{S} - \hat{\mathbf{S}}\|_F \\ &= \sigma_{\max}(\mathbf{H}) \|\Theta - \hat{\Theta}\|_F. \end{aligned} \quad (42)$$

Theorem 2 indicates $\delta_{\gamma'k}^* \leq 1/3$ as the sufficient condition for the sparse source recovery. In the following we investigate the implication of this condition for the previously mentioned acquisition schemes to bound the number of CS measurements.

1) *Dense Random Sampling:* Assume the compression matrix A that is used for subsampling data in (2) is an $m \times n_1 n_2$ matrix whose elements are drawn independently at random from the Gaussian, Bernoulli or subgaussian distributions. According to Remark 1, such matrices satisfy D-RIP adapted to Φ (with the constant $\delta_{\gamma'k}^* \leq 1/3$) provided by:

$$m \gtrsim \gamma' k \log(\rho n_1 / \gamma' k). \quad (43)$$

2) *Uniform Random Sampling:* The same type of analysis indicates a very poor performance for the uniform random acquisition scheme described in section III-B2. The corresponding sampling matrix has a block-diagonal form $A = \text{Id}_{n_2} \otimes \tilde{A}$. Here, we assume that the core compression matrix \tilde{A} that separately applies to each channel is an $\hat{m} \times n_1$ matrix whose elements are drawn independently at random from Gaussian, Bernoulli or subgaussian distributions.

According to the theoretical analysis provided in section IV-A, the sufficient condition for source recovery via (12) is $\delta_k(A) \leq \frac{\sqrt{2} - 1 - \delta_k(\Phi')}{1 + \delta_k(\Phi')}$ which, by considering (36) can be rephrased as:

$$\delta_k(A) \leq \frac{\sqrt{2} - 1 - \eta}{1 + \eta}. \quad (44)$$

For a compression matrix with this structure and by using Lemma 1 we can deduce $\delta_k(A) \leq \delta_k(\tilde{A})$. Now similarly as for the bound (26), \tilde{A} satisfies the RIP with the constant above (and so does A) as long as $\hat{m} \geq c k \log(n_1/k)$ or equivalently,

$$m \geq c n_2 k \log(n_1/k). \quad (45)$$

The constant c depends on the conditioning of the mixture matrix \mathbf{H} . When the columns of \mathbf{H} are very coherent, the extreme singular values spread away from each other and η becomes large. As a consequence, \tilde{A} (or equivalently A) must

⁴As for $\gamma'k \geq n_1 n_2$ an $n_1 n_2 \times n_1 n_2$ identity matrix A always satisfies $\delta_{\gamma'k}^* = 0$ (i.e. there is no advantage by replacing the full Nyquist sampling with CS), Theorem 2 becomes useful only when we have $\gamma'k < n_1 n_2$ which for the value of γ' in the theorem implies $\xi(\mathbf{H}) \leq \sqrt{\frac{n_1 n_2 / k - 1}{2}}$.

| CS Acquisition Scheme | Dense | Dense | Uniform | Decorrelating |
|----------------------------------|----------------------------------|-----------------------------------|----------------------------------|-----------------------------------|
| CS Recovery Approach | BPDN | SS- ℓ_1 | SS- ℓ_1 | SS- ℓ_1 |
| CS measurements $m \gtrsim$ | $\mathcal{O}(n_2 k \log(n_1/k))$ | $\mathcal{O}(k \log(\rho n_1/k))$ | $\mathcal{O}(n_2 k \log(n_1/k))$ | $\mathcal{O}(k \log(\rho n_1/k))$ |
| Constant depends on \mathbf{H} | - | Yes | Yes | No |

TABLE I: Measurement bounds for random sampling schemes: dense, uniform and decorrelating, and for recovery approaches: BPDN and SS- ℓ_1 (i.e. source separation based recovery using (12) or (21)). The last row shows whether the bounds for the SS- ℓ_1 are sensitive to the conditioning of the mixing matrix \mathbf{H} .

satisfy RIP for a smaller constant which, as discussed earlier in section IV-A, implies c to be large and more CS measurements are required for source recovery.

3) *Decorrelating Random Sampling*: When a decorrelation step is incorporated into the compressive acquisition process, \mathbf{H} is discarded in the recovery formulation, and then we can use the standard RIP analysis in [3], [4] to evaluate the source recovery performance. Therefore, if $A = \text{Id}_\rho \otimes \tilde{A}$ satisfies the RIP with a constant $\delta_k(A) \leq \sqrt{2} - 1$, then the solution $\hat{\Theta}$ to (21) obeys the following error bound:

$$\|\Theta_{vec} - \hat{\Theta}_{vec}\|_2 \leq c_0 k^{-1/2} \|\Theta_{vec} - (\Theta_{vec})_k\|_1 + c_1 \varepsilon, \quad (46)$$

where the constants c_0, c_1 are the same as in (23).

Now, since A is a block diagonal matrix, we can proceed along the exact same steps as for the uniform sampling scheme (Section IV-C2) to bound the minimum number of CS measurements such that A satisfies the RIP:

$$\hat{m} \geq \bar{c} k \log(n_1/k). \quad (47)$$

Unlike the previous measurement bounds for the non-decorrelating sampling schemes, here \bar{c} is a fixed constant independent of the mixture matrix \mathbf{H} . Consequently, the total number of CS measurements used for source recovery is:

$$m \geq \bar{c} \rho k \log(n_1/k). \quad (48)$$

Note that, for a noiseless sampling scenario ($\varepsilon = 0$) the minimization (21) can be decoupled into ρ independent ℓ_1 minimizations, each of them corresponding to a sparse recovery of a certain source. Now, if we assume that each source has exactly $k' = k/\rho$ nonzero coefficients, then a perfect recovery can be guaranteed as long as $\delta_{k'}(\tilde{A}) \leq \sqrt{2} - 1$ which, for a matrix \tilde{A} drawn from the previously-mentioned distributions, implies that $\hat{m} \geq \bar{c} k' \log(n_1/k')$ and consequently:

$$m = \rho \hat{m} \geq \bar{c} k \log(\rho n_1/k). \quad (49)$$

Compared to (48) where m is roughly proportional to ρk , here the measurement bound improves by a factor ρ and it is mainly proportional to the sparsity level k of all sources.

D. Conclusions on the Theoretical Bounds

Consider a multichannel data derived by the linear mixture (9) of ρ sources, each having a k' -sparse representation i.e. \mathbf{S} is $k = \rho k'$ sparse. Table I summarizes the scaling-orders of the number of CS measurements sufficient for an exact data reconstruction for different noiseless random acquisition schemes and sparse recovery approaches. As we can observe, compressed sensing via source recovery using (12) once it is coupled with a proper CS acquisition (i.e., Dense i.i.d.

subgaussian A , or a random decorrelating sampling scheme as in sections III-B1 and III-B3) leads to a significantly improved bound compared to standard methods such as BPDN. More remarkably, the number of CS measurements turns out to be independent of the number n_2 of channels.

Finally note that the measurement bound for the source-separation-based reconstruction approach, which uses a non-decorrelating random compression matrix, depends on the conditioning of the mixture parameters via the constant factor γ' in (43). Therefore, when the columns of \mathbf{H} are highly coherent, the condition number of \mathbf{H} becomes relatively large, and so does γ' . This limitation can be circumvented thanks to the decorrelating acquisition scheme.

V. APPLICATIONS IN COMPRESSIVE HYPERSPECTRAL IMAGERY

Compressed sensing is particularly promising for hyperspectral imagery where the acquisition procedure is very costly. This type of images can be approximated by a linear mixture model as in (9) where each spatial pixel is populated with a very few number of materials (i.e. sources). In this regard, $\mathbf{S} \in [0, 1]^{n_1 \times \rho}$ is a matrix whose ρ columns are *source images* (vectorized 2D images) indicating the percentage of each material in one of the n_1 spatial pixels, and therefore

$$\sum_{j=1}^{\rho} [\mathbf{S}]_{i,j} = 1 \quad \forall i \in \{1, \dots, n_1\}. \quad (50)$$

Moreover, $\mathbf{H} \in \mathbb{R}_+^{n_2 \times \rho}$ is a matrix whose columns contain the spectral signatures of the corresponding sources of \mathbf{S} . Note that in some particular applications and specially when the spatial resolution is high enough, the source images become *disjoint*, meaning that each spatial pixel contains only one material and $[\mathbf{S}]_{i,j} \in \{0, 1\}$.

The two key priors that will be essential for compressive source identification are the following: i) Each source image contains piecewise smooth variations along the spatial domain, implying a sparse representation in a wavelet basis, or sparsity of its gradient, and ii) each spatial pixel is a non-negative linear combination of a *small* number of sources.

In the next two sections we introduce two classes of source separation based recovery approaches that are particularly adapted to hyperspectral compressive imagery.

A. Compressive HSI Source Separation via Convex Minimization

According to our earlier assumptions, source images are spatially piecewise smooth, which means the coefficients Θ of $\mathbf{S} = \Psi_{2D} \Theta$ are sparse in a 2-dimensional wavelet basis

$\Psi_{2D} \in \mathbb{R}^{n_1 \times n_1}$. We conveniently rephrase this representation in a vectorized form $\mathbf{S}_{vec} = \Psi \Theta_{vec}$ with $\Psi = \text{Id}_\rho \otimes \Psi_{2D}$ as described in Section II-B.

Taking into account the sparsity of Θ_{vec} and by incorporating specific assumptions such as (50) and non-negativity we can extend the ℓ_1 minimization approach in (12) as follows:

$$\begin{aligned} & \arg \min_{\Theta} \|\Theta_{vec}\|_1 & (51) \\ \text{subject to} & \|y - A\Phi\Psi\Theta_{vec}\|_2 \leq \varepsilon \\ & \Psi_{2D}\Theta\mathbb{I}_\rho = \mathbb{I}_{n_1} \\ & \Psi\Theta_{vec} \geq 0. \end{aligned}$$

Where, \mathbb{I}_n denotes an all one n -dimensional vector. The first constraint is the same as the fidelity constraint in (12). The last two constraints impose the element-wise non-negativity of \mathbf{S} and the ‘‘percentage’’ normalization (50) *i.e.*, each row of \mathbf{S} belongs to the positive face of the simplex in \mathbb{R}^ρ . Minimizing the ℓ_1 norm together with the last two constraints (that is equivalent to an additional ℓ_1 norm constraint) gives solutions that contain both desired sorts of sparsity: i) along the 2D wavelet coefficients of \mathbf{S} and, ii) along each row of \mathbf{S} .

Note that the theoretical analysis given in Section IV-C can also apply here to bound the performance of (51). Although we bound the error similarly as for (12), one can naturally expect a much better performance for (51) thanks to the two additional constrains.

Alternatively, we can formulate problem (51) in a general ‘‘analysis’’ formulation with an analysis sparsity prior $\mathcal{P}(\mathbf{S})$:

$$\begin{aligned} & \arg \min_{\mathbf{S}} \mathcal{P}(\mathbf{S}) & (52) \\ \text{subject to} & \|y - A\Phi\mathbf{S}_{vec}\|_2 \leq \varepsilon \\ & \mathbf{S}\mathbb{I}_\rho = \mathbb{I}_{n_1} \\ & \mathbf{S}_{vec} \geq 0. \end{aligned}$$

which is equivalent to (51) when $\mathcal{P}(\mathbf{S}) = \|\Psi^*\mathbf{S}_{vec}\|_1$ and Ψ is a square and invertible operator. Another efficient analysis prior for image regularization is the Total Variation which can be applied on each source image of the HSI with the prior: $\mathcal{P}(\mathbf{S}) = \sum_j \|\mathbf{S}_j\|_{TV}$. The problem formulation (52) is general and includes the decorrelating schemes discussed in sections III-B1 and III-B3. Indeed inserting the matrix A of (14) in (52) leads to the following fidelity term $\|y - \tilde{A}_\rho \mathbf{S}_{vec}\|_2 \leq \varepsilon$ while the other terms remain unchanged.

In the next Section we provide an iterative algorithm for solving problem (52). When sources are disjoint, it is also possible to add a *hard thresholding* post-processing step that sets the maximum coefficient of each row of $\hat{\mathbf{S}}$ equal to one and set to zero the other coefficients.

B. The PPXA Algorithm for Compressive Source Separation

The Parallel Proximal Splitting Algorithm (PPXA) [28] is an iterative method for minimizing an arbitrarily finite sum of lower semi-continuous (l.s.c.) convex functions.⁵ Each of

⁵Note that, similarities between PPXA and another popular convex optimization scheme of Alternating Direction Method of Multipliers (ADMM) is explained, for instance, in [29].

Algorithm 1: Parallel Proximal Algorithm to solve (52).

Input: $y, A, \Phi, \varepsilon, \beta > 0$.

Initializations:

$n = 0, \mathbf{S}_0 = \Gamma_{1,0} = \Gamma_{2,0} = \Gamma_{3,0} \in \mathbb{R}^{n_1 \times n_2}$

repeat

for $(i = 1 : 3)$ **do**

$P_{i,n} = \text{prox}_{3\beta f_i}(\Gamma_{i,n})$

end

$\mathbf{S}_{n+1} = (P_{1,n} + P_{2,n} + P_{3,n})/3$

for $(i = 1 : 3)$ **do**

$\Gamma_{i,n+1} = \Gamma_{i,n} + 2\mathbf{S}_{n+1} - \mathbf{S}_n - P_{i,n}$

end

until convergence;

the iteration consists in computing the *proximity* operator of all functions (which can be done in parallel), averaging their results and updating the solution until convergence. The proximity operator of a function $f(x) : \mathbb{R}^n \rightarrow \mathbb{R}$ is defined as $\text{prox}_f : \mathbb{R}^n \rightarrow \mathbb{R}^n$ [28]:

$$\arg \min_{\tilde{x} \in \mathbb{R}^n} f(\tilde{x}) + \frac{1}{2} \|x - \tilde{x}\|_2^2. \quad (53)$$

For solving (52) with PPXA, we rewrite it as the minimization of the sum of three l.s.c. convex functions:

$$\arg \min_{\mathbf{S}} f_1(\mathbf{S}) + f_2(\mathbf{S}) + f_3(\mathbf{S}), \quad (54)$$

with $f_1(\mathbf{S}) = \mathcal{P}(\mathbf{S})$, $f_2(\mathbf{S}) = i_{\mathcal{B}_2}(\mathbf{S})$ and $f_3(\mathbf{S}) = i_{\mathcal{B}_{\Delta+}}(\mathbf{S})$ and where $i_{\mathcal{C}}$ is the indicator function of a convex set \mathcal{C} defined as:

$$i_{\mathcal{C}}(\mathbf{S}) = \begin{cases} 0 & \text{if } \mathbf{S} \in \mathcal{C} \\ +\infty & \text{otherwise,} \end{cases} \quad (55)$$

and the convex sets $\mathcal{B}_2, \mathcal{B}_{\Delta+} \subset \mathbb{R}^{n_1 \times \rho}$ are respectively, the set of matrices that satisfy the fidelity constraint $\|y - A\Phi\mathbf{S}_{vec}\|_2 \leq \varepsilon$, and the set of matrices whose rows belong to the standard simplex in \mathbb{R}^ρ . The template of the PPXA algorithm that solves (54) and hence (52) is given in Algorithm 1. We now derive the proximity operator of each function f_i . Note that the definition of the proximity operator in (53) naturally extends for matrices by replacing the ℓ_2 norm with the Frobenius norm.

For $\mathcal{P}(\mathbf{S}) = \|\Psi^*\mathbf{S}_{vec}\|_1$, a standard calculation shows that

$$(\text{prox}_{\alpha \mathcal{P}})_i = \text{sign}((\Psi^*\mathbf{S}_{vec})_i) \cdot (|(\Psi^*\mathbf{S}_{vec})_i| - \alpha)_+, \quad (56)$$

which is the *soft thresholding* operator applied on the wavelet coefficients of \mathbf{S} . The proximity operator of $\mathcal{P}(\mathbf{S}) = \sum_{j=1}^{\rho} \|\mathbf{S}_j\|_{TV}$ can be decoupled and computed in parallel for each of the ρ sources via an efficient implementation proposed by [30]. By definition, the proximal operator of an indicator function $i_{\mathcal{C}}(\mathbf{S})$ is the orthogonal projection of \mathbf{S} onto the corresponding set \mathcal{C} . The projection onto the standard simplex $\mathcal{B}_{\Delta+}$ can be done in one iteration using the method proposed by Duchi et al. [31]. For a general implicit operator $L \triangleq A\Phi$, the projector onto \mathcal{B}_2 can be computed using a *forward backward* scheme as proposed in [32]. This projection usually has the dominant computational complexity of the algorithm because of costly sub-iterations. However if the

Algorithm 2: Iterative Hard Thresholding Algorithm to approximate solution of (58)

Input: $y, A, \Phi, \gamma = 1/\|A\Phi\Psi\|^2 = 1/\|A\Phi\|^2$ and k .

Initializations:

$n = 0, \Theta^0 \in \mathbb{R}^{n_1 \times \rho}$

repeat

1- Gradient descent:

$$\Theta_{vec}^{n+1} = \Theta_{vec}^n - \gamma \nabla F(\Theta^n)$$

2- Hard thresholding:

$$\Theta_{vec}^{n+1} = \text{Th}_k(\Theta_{vec}^{n+1})$$

3- Orthogonal matrix procrustes:

$$\text{Update } \Omega : [\Omega]_{i,i} = \sqrt{n_1} \frac{\|\Theta_{.,i}^{n+1}\|_2}{\|\Theta_{.,i}^{n+1}\|_F}$$

$$\text{Singular value decomposition: } U\Sigma V^* = \Theta^{n+1}\Omega$$

$$\Theta^{n+1} = UV^*\Omega$$

4- Simplex projection:

$$\Theta^{n+1} = \Psi_{2D}^* \text{Project}_{\mathcal{B}_{\Delta+}}(\Psi_{2D}\Theta^{n+1})$$

until convergence;

decorrelating sampling scheme is used and $L = \tilde{A}_\rho$ is a tight frame (i.e., $\forall x \in \mathbb{R}^m \ LL^*x = \nu x$ for a constant ν), then according to the *semi-orthogonal linear transform* property of proximity operators [28], the orthogonal projection onto \mathcal{B}_2 has the following explicit form:

$$(\text{prox}_{\alpha f_2}(\mathbf{S}))_{vec} = \mathbf{S}_{vec} + \frac{1}{\nu} (\tilde{A}_\rho)^* \mathbf{r} \left(1 - \frac{\varepsilon}{\|\mathbf{r}\|_2} \right)_+, \quad (57)$$

with $\mathbf{r} = y - \tilde{A}_\rho \mathbf{S}_{vec}$.

C. Compressive HSI Source Separation via Iterative Hard Thresholding

If the source images are disjoint, the following non-convex minimization can be alternatively used for recovering the sparse wavelet coefficients of the sources:

$$\begin{aligned} \arg \min_{\Theta} \quad & \|y - A\Phi\Psi\Theta_{vec}\|_2^2 & (58) \\ \text{subject to} \quad & \|\Theta_{vec}\|_0 \leq k \\ & \text{Off diag}(\Theta^* \Theta) = 0 \\ & \Psi_{2D} \Theta \mathbb{I}_\rho = \mathbb{I}_{n_1} \\ & \Psi \Theta_{vec} \geq 0. \end{aligned}$$

where the operator $\text{Off diag}(B)$ returns the off-diagonal elements of matrix B , and the ℓ_0 norm constraint on Θ_{vec} imposes the wavelet coefficients to be k -sparse. The second constraint imposes the orthogonality of the wavelet coefficients which is a consequence of the source disjointness. The two last constraints are the same as in (51).

Despite its convex objective term, (58) has multiple non-convex constraints and is therefore a non-convex problem. We propose an algorithm similar to the *Iterative Hard Thresholding* (IHT) algorithm [20] to approximate the solution of (58). At each iteration the current solution is updated by a gradient descent step followed by a hard thresholding step $\text{Th}_k(\cdot)$ that selects the k largest wavelet coefficients of Θ_{vec} . In addition the three last constraints of (58) are applied sequentially:

- First, a procedure inspired by the *orthogonal matrix procrustes* is applied to diagonalize $\hat{\Theta}^* \hat{\Theta}$. Let Ω be a $\rho \times \rho$ diagonal matrix where for $1 \leq i \leq \rho$ we have

$$[\Omega]_{i,i} = \sqrt{n_1} \frac{\|\hat{\Theta}_{.,i}\|_2}{\|\hat{\Theta}\|_F}. \quad (59)$$

Since for disjoint sources we have $\|\mathbf{S}\|_F = \|\Theta\|_F = \sqrt{n_1}$, then a good orthogonal matrix that would approximate $\hat{\Theta}$ and keeps the energy of the current estimate of each source image proportional to that of the previous estimate would be $UV^*\Omega$ through the following singular value decomposition $U\Sigma V^* = \hat{\Theta}\Omega$.

- Second, the current solution $\hat{\mathbf{S}} = \Psi_{2D} \hat{\Theta}$ is projected onto the standard simplex as in [31].

The description of this algorithm can be found in Algorithm 2. Note that the gradient of the objective functional $F(\Theta) = \|y - A\Phi\Psi\Theta_{vec}\|_2^2$ is:

$$\nabla F(\Theta) = -(A\Phi\Psi)^*(y - A\Phi\Psi\Theta_{vec}). \quad (60)$$

Using the decorrelating scheme, the objective function in (58) becomes $F(\Theta) = \|y - \tilde{A}_\rho \Psi \Theta_{vec}\|_2^2$ with gradient :

$$\nabla F(\Theta) = -(\tilde{A}_\rho \Psi)^*(y - \tilde{A}_\rho \Psi \Theta_{vec}). \quad (61)$$

The rest of Algorithm 2 remains unchanged.

VI. EXPERIMENTS

In this section, we evaluate the capability of the methods presented in Section V, (called “*SS methods*” and summed up in table II) to separate the sources and recover HSI in various scenarios: various noise levels (from noiseless to 10 dB SNR), various sampling ratios (from $m/(n_1 n_2) = 1/4$ to $1/32$ sampling rates), various sampling mechanisms (uniform and dense sampling), on three different HSI (Geneva, Pavia and Urban). We also compare the *SS methods* with the classical methods for CS, such as the BPDN problem (7) BPDN, the TVDN problem (8) TVDN, both solved with a Douglas-Rachford (DR) splitting algorithm [33].

A. Sampling Mechanism

We used two different sampling schemes: i) the sensing matrix A is *dense* (and the methods implementing the decorrelation step cannot be applied), and ii) *uniform* sampling where the sensing matrix is block diagonal with identical blocks as in (17). In the latter, the decorrelation step can be applied as explained in section III-B. So as to generate the random sampling matrices A and \tilde{A} that can be used in practical applications, we used the Random Convolution (RC) measurement scheme proposed by Romberg [34] that convolves the image with a random pattern using few optical blocks. More remarkably, sampling matrices generated by RC are tight frames and thus for decorrelating schemes, they benefit from a closed form expression (57) for computing $\text{prox}_{\alpha f_2}(\cdot)$ that can massively accelerate the recovery procedure.

TABLE II: Description of the proposed *SS methods*.

| Method name | Description |
|---------------|--|
| SS-IHT | Problem (58) solved with Algorithm 2 with gradient $\nabla F(\Theta)$ of Eq. (60). |
| SS-l1 | Problem (52) solved with Algorithm 1, with $\mathcal{P}(\mathbf{S}) = \ \Psi^* \mathbf{S}_{vec}\ _1$ and $prox_{\alpha f_2}(\cdot)$ computed using a forward-backward scheme as proposed in [32]. |
| SS-TV | Problem (52) solved with Algorithm 1, with $\mathcal{P}(\mathbf{S}) = \sum_{j=1}^p \ \mathbf{S}_j\ _{TV}$ and $prox_{\alpha f_2}(\cdot)$ computed using a forward-backward scheme as proposed in [32]. |
| SS-IHT-decorr | Problem (58) solved with Algorithm 2 with gradient $\nabla F(\Theta)$ of Eq. (61). |
| SS-l1-decorr | Problem (52) solved with Algorithm 1, with $\mathcal{P}(\mathbf{S}) = \ \Psi^* \mathbf{S}_{vec}\ _1$, and $prox_{\alpha f_2}(\cdot)$ computed with the closed form Eq. (57). |
| SS-TV-decorr | Problem (52) solved with Algorithm 1, with $\mathcal{P}(\mathbf{S}) = \sum_{j=1}^p \ \mathbf{S}_j\ _{TV}$ and $prox_{\alpha f_2}(\cdot)$ computed with (57). |

TABLE III: Performances of *SS methods* (presented in Table II) and the classical BPDN, TVDN methods, for different noise levels and subsampling ratios, tested on Geneva HSI: Source separation Accuracy after hard thresholding post-processing (left), HSI reconstruction SNR before post-processing (right). Methods with the highest accuracy are highlighted in each column, and the reconstruction SNRs higher than 60 dB are marked as $+\infty$.

| Sampling SNR | $+\infty$ dB | | | | 30 dB | | | | 10 dB | | | |
|-----------------------------------|------------------------|------------------------|------------------------|------------------|------------------------|------------------------|------------------------|------------------|------------------|------------------|-------------------|-------------------|
| | 1/4 | 1/8 | 1/16 | 1/32 | 1/4 | 1/8 | 1/16 | 1/32 | 1/4 | 1/8 | 1/16 | 1/32 |
| SS-IHT(<i>dense sampling</i>) | 0.69 10.5 | 0.61 8.3 | 0.57 7.4 | 0.48 6.6 | 0.71 10.5 | 0.6 8 | 0.57 7.3 | 0.48 6.6 | 0.71 10.4 | 0.6 8.1 | 0.57 7.2 | 0.48 6.6 |
| SS-l1(<i>dense sampling</i>) | 1.0 $+\infty$ | 1.0 40.6 | 0.95 19.0 | 0.81 12.8 | 1.0 $+\infty$ | 1.0 39.9 | 0.95 18.9 | 0.8 12.8 | 1.0 37.8 | 0.98 24.3 | 0.91 15.2 | 0.73 11.5 |
| SS-TV(<i>dense sampling</i>) | 1.0 $+\infty$ | 1.0 56.5 | 1.0 29.7 | 0.92 15.0 | 1.0 $+\infty$ | 1.0 56.5 | 1.0 29.5 | 0.91 15.0 | 1.0 40.4 | 1.0 32.6 | 0.98 22.2 | 0.88 13.9 |
| BPDN(<i>dense sampling</i>) | - 20.8 | - 17.1 | - 14.5 | - 12.4 | - 20.0 | - 17.0 | - 14.6 | - 12.6 | - 14.2 | - 12.9 | - 11.6 | - 10.4 |
| TVDN(<i>dense sampling</i>) | - 41.1 | - 29.9 | - 24.0 | - 19.0 | - 30.6 | - 26.7 | - 22.1 | - 18.4 | - 18.0 | - 16.6 | - 14.8 | - 14.0 |
| SS-IHT(<i>uniform sampling</i>) | 0.43 6.8 | 0.38 5.9 | 0.31 5.2 | 0.25 4.9 | 0.43 6.7 | 0.37 5.9 | 0.31 5.2 | 0.26 4.8 | 0.43 6.8 | 0.37 6.0 | 0.3 5.2 | 0.26 4.8 |
| SS-l1(<i>uniform sampling</i>) | 0.97 17.9 | 0.73 9.9 | 0.45 7.0 | 0.31 6.0 | 0.95 17.8 | 0.73 9.9 | 0.48 7.0 | 0.3 6.0 | 0.96 17.7 | 0.75 9.9 | 0.42 7.0 | 0.3 6.0 |
| SS-TV(<i>uniform sampling</i>) | 1.0 32.9 | 0.98 21.5 | 0.9 14.6 | 0.76 10.8 | 1.0 32.9 | 0.97 21.5 | 0.89 14.6 | 0.74 10.8 | 1.0 32.0 | 0.97 21.2 | 0.88 14.5 | 0.74 10.8 |
| BPDN(<i>uniform sampling</i>) | - 20.7 | - 16.9 | - 14.4 | - 12.3 | - 19.9 | - 16.8 | - 14.5 | - 12.5 | - 14.2 | - 12.9 | - 11.6 | - 10.3 |
| TVDN(<i>uniform sampling</i>) | - 41.2 | - 31.4 | - 23.7 | - 18.9 | - 30.7 | - 24.9 | - 21.9 | - 18.3 | - 18.2 | - 16.4 | - 15.1 | - 14.0 |
| SS-IHT-decorr | 0.98 22.1 | 0.98 20.1 | 0.96 18.3 | 0.94 16.0 | 0.99 22.2 | 0.98 20.2 | 0.96 18.3 | 0.94 15.9 | 0.98 20.9 | 0.97 19.4 | 0.95 17.6 | 0.92 15.6 |
| SS-l1-decorr | 1.0 52.0 | 0.99 25.9 | 0.97 18.9 | 0.92 15.0 | 1.0 40.6 | 0.99 24.4 | 0.96 18.4 | 0.91 14.9 | 0.98 20.2 | 0.95 17.2 | 0.92 15.0 | 0.87 12.7 |
| SS-TV-decorr | 1.0 $+\infty$ | 1.0 $+\infty$ | 1.0 $+\infty$ | 1.0 33.1 | 1.0 $+\infty$ | 1.0 $+\infty$ | 1.0 $+\infty$ | 1.0 29.8 | 1.0 32.3 | 0.99 24.4 | 0.98 19.9 | 0.96 17.7 |

B. The Geneva HSI

Geneva HSI is semi-synthetic and is constructed by selecting six spectra (i.e. columns of \mathbf{H}) from the USGS digital spectral library⁶, and multiplying them by source maps that have been annotated by experts on the basis of images of a rural suburb of Geneva.⁷ The HSI cube has spatial slices of the resolution $N = 256 \times 256$ that are taken over $J = 224$ frequency bands. We test different methods on this dataset, for different sampling rates and different noise levels, and we report their performances in Table III. Since source images are disjoint, we apply the hard thresholding post-processing (see Section V-A) to all SS methods, and we measure the *source recovery* quality in terms of *accuracy* indicating the percentage of correctly classified pixels in the spatial domain. Meanwhile and to contrast the influence of post-processing, we use the estimated sources before post-processing for *HSI recovery* and we report the quality in terms of *reconstruction SNR*. Figure 1 illustrates the recovered sources (before post-processing) of different *SS methods* for various sampling schemes (dense, uniform, decorrelating). We observe in Tab. III that for methods achieving reconstruction SNRs higher than 29 dB, adding

the post-processing step boosts their performances, and results in an exact reconstruction (indicated by the Accuracy = 1).

1) *HSI reconstruction performances of the SS methods*: We observe in Tab. III that

- Dense sampling scheme is always better than the uniform sampling scheme.
- Decorrelated scheme is almost always better than dense sampling (except for the ℓ_1 -based method).
- SS-TV-decorr results in perfect reconstruction in the cases where the sampling ratio is higher or equal to 1/16 and performs better than all the other methods in all regimes, except in high noise of 10 dB SNR, where SS-TV (using dense sampling) performs slightly better.

2) *Comparison with Classical CS Methods*: We observe that SS-TV-decorr always obtains significantly better results than the classical CS methods in all regimes.

3) *Source Recovery Accuracy*: We observe in Tab. III that SS-TV-decorr based on TV regularization and decorrelation, which achieves the best performance for HSI reconstruction, also obtains the best performance for source separation. Fig. 1 also indicates that decorrelating schemes give better unmixed source images, prior to the post-processing step.

⁶ Available online <http://speclab.cr.usgs.gov/spectral.lib06>.

⁷ This dataset is available at <http://infoscience.epfl.ch/record/180911>. We acknowledge Xavier Gigandet and Meritxell Bach Cuadra for providing this ground truth map.

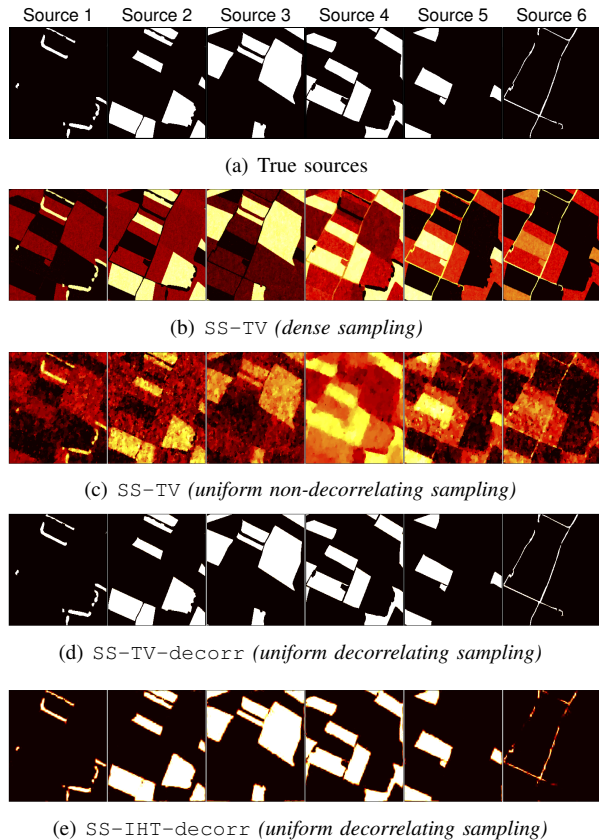


Fig. 1: Estimated source images of Geneva HSI for different sampling schemes and recovery methods (subsampling ratio: 1/16, noiseless sampling, no post-processing).

C. The Pavia HSI

In this part we consider a real-world HSI of resolution $N = 1024 \times 512$, $J = 102$, captured over the city center of Pavia (Italy).⁸ Figures 2(a)-(b) show the scene and the ground truth of five underlying sources in the foreground pixels. We apply the pre-described compressive sampling schemes to acquire the whole HSI (including both foreground and background pixels). Having the ground truth map, we use the least square approximation to get the spectral signatures of all sources i.e. $\mathbf{H} = (S_{\mathcal{M}}^T S_{\mathcal{M}})^{-1} S_{\mathcal{M}}^T X_{\mathcal{M}}$, where \mathcal{M} is the index set of the foreground pixels. We then used these estimated spectra for our SS methods in order to classify the foreground pixels, directly in compressed domain (separation and classification problems are equivalent for spatially disjoint sources). For this we simply modify the simplex projection constraints (i.e., $\mathbf{S} \mathbb{I}_{\rho} = \mathbb{I}_{n_1}$) in both convex (52) and non-convex (58) approaches so that, it performs only on the foreground pixels and we set the background pixels to zero i.e. $\sum_{j=1}^{\rho} [\mathbf{S}]_{i,j} = 1 \forall i \in \mathcal{M}$, and $[\mathbf{S}]_{i,j} = 0 \forall j, \forall i \notin \mathcal{M}$.

Note that our SS methods are facing the following challenges for classifying this image: first, compressive acquisition systems give measurements that are globally merging both background and foreground pixels, and thus recovering only the foreground pixels (and setting the background to zero

⁸This dataset has been used for classification evaluation (using fully sampled image) in 2008 GRS-S Data Fusion Contest [35], and we thank Devis Tuia for providing us with the ground truth map.

TABLE IV: Classification accuracy of SS methods in Tab. II (after hard thresholding post-processing) tested on PAVIA HSI.

| Sampling rate | 1/4 | 1/8 | 1/16 | 1/32 |
|------------------------|------|------|------|------|
| SS-IHT(dense sampling) | 0.57 | 0.56 | 0.56 | 0.55 |
| SS-l1(dense sampling) | 0.88 | 0.85 | 0.8 | 0.74 |
| SS-TV(dense sampling) | 0.95 | 0.94 | 0.93 | 0.91 |
| SS-IHT-decorr | 0.84 | 0.79 | 0.73 | 0.64 |
| SS-l1-decorr | 0.84 | .8 | 0.75 | 0.69 |
| SS-TV-decorr | 0.92 | .92 | 0.91 | 0.9 |

in (52) and (58)) from the CS measurements means that the contribution of the background pixels is considered as a noise with a considerable energy. Second, pixels within the same class do not share exactly the same spectrum, and their deviations from the approximated \mathbf{H} is relatively high i.e. $\|X_{\mathcal{M}} - S_{\mathcal{M}} \mathbf{H}^T\|_F / \|X_{\mathcal{M}}\|_F \sim 28\%$. As a result, the mixture model (9) does not exactly hold. We account for these mismatches using the sampling noise model defined in (2).

a) *Results:* We evaluate the classification performances of our SS methods for dense and decorrelating sampling schemes, and for different sampling rates. We measure the overall classification accuracies and report them in Table IV. Figures 2(c)-(h) show the resulting classification maps for different recovery methods. Note that both the figures and table include our results after the hard thresholding post-processing step. We observe that the TV-based methods outperform other schemes, and they are capable to achieve accuracies higher than 90% for all tested sampling rates. Remarkably, we observe that decorrelating sampling leads to a comparable (for TV and ℓ_1 -based methods) or a better (for IHT) performance with respect to dense sampling, indicating the robustness of the decorrelation step against a strong model mismatch. In Section VI-E2 we discuss that this robustness comes with a huge computational advantage as well.

D. The Urban HSI

We test our methods on the real-world Urban HSI ($N = 256 \times 256$, $J = 171$) with spatially mixed (non-disjoint) sources.⁹ As the ground truth of this image (i.e., the true source images and their corresponding spectral signatures) is not available, we first separate the underlying sources using a *blind* source separation algorithm for fully-sampled HSI [14] and later, use these separated sources, depicted in Fig. 3(a), as a reference. Figure 3 demonstrates the reconstructed sources of Urban using our proposed SS approaches based on convex minimization, for different noiseless sampling mechanisms (dense, uniform, uniform-decorrelating) and for a fixed subsampling ratio.¹⁰ Moreover, Figure 4 shows the reconstructed Urban HSI for a certain spectral band, using the source images estimated by the SS methods based on TV minimization (i.e., SS-TV and SS-TV-decorr) as well as the baseline TVDN.

b) *Results:* Similar to our previous experiment, we observe that for a uniform (non-decorrelating) sampling scheme SS-TV has very poor recovery performance. Meanwhile, adding a decorrelation step results in a significant improvement in source recovery. As we can see in Figure 3(b), the

⁹Available online <http://www.agc.army.mil/hypercube>.

¹⁰Since sources of Urban are not spatially disjoint, we do not apply Algo.2.

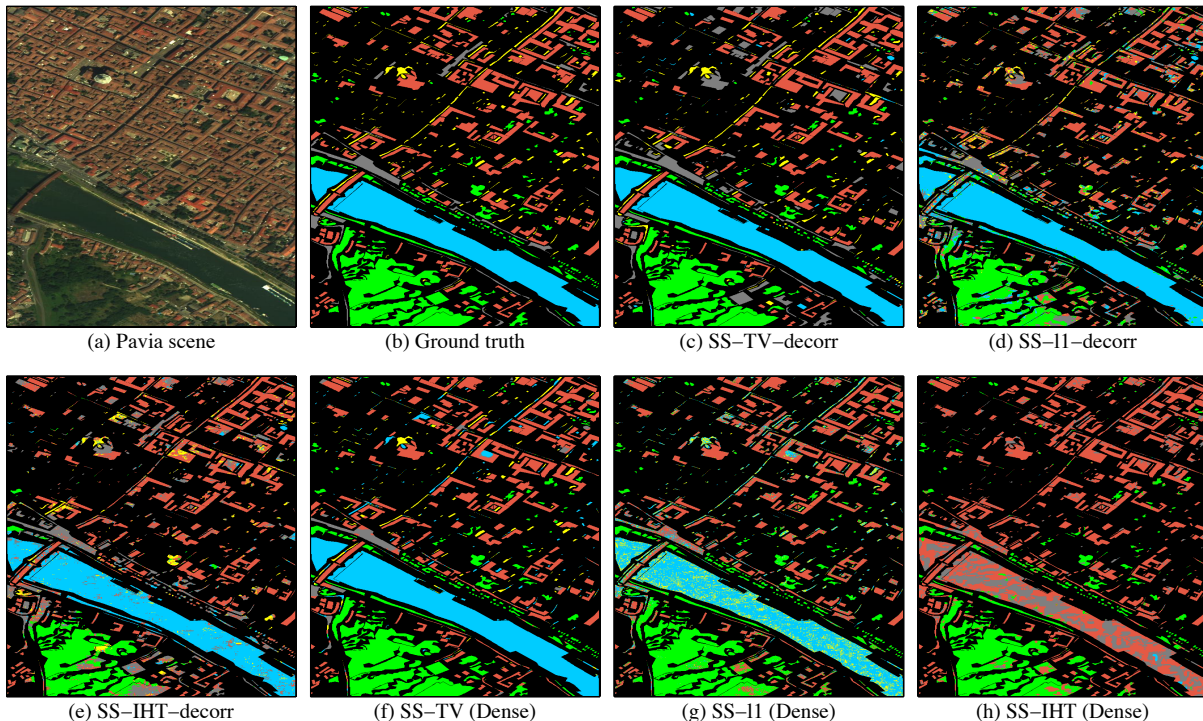


Fig. 2: Compressive classification of Pavia HSI using SS methods (with hard thresholding post-processing) for dense and uniform decorrelating sampling schemes (subsampling ratio: 1/16). Classification maps contain five classes on foreground pixels namely roads (gray), water (blue), vegetation (green), shadows (yellow), buildings (red), and the background pixels are marked in black.

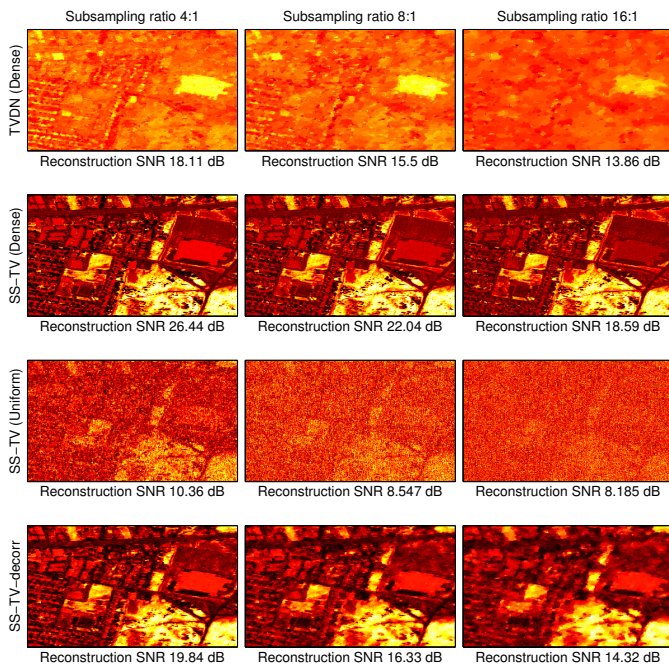


Fig. 4: Reconstructed Urban HSI at band 33, using TVDN and TV-based SS methods for various sampling schemes (dense, uniform non-decorrelating, uniform decorrelating) and subsampling ratios.

estimated source images using SS-TV for a dense sampling scheme have better spatial resolutions, but are not as well separated as with the SS-TV-decorr method. Finally, we can observe in Figure 4 that the SS-methods (except uniform non-decorrelating) considerably outperform the baseline TVDN in terms of reconstruction quality.

E. Conclusion on the Experiments

1) *Recovery Performance*: Decorrelation step is of great benefit and the proposed method SS-TV-decorr, based on TV regularization and decorrelation, performs the best for HSI reconstruction and source estimation for almost all tested sampling rates and SNR regimes.

2) *Computational Performance*: We ran all the codes on a MacBook Pro 2.3 GHz Intel CPU, 8 GB RAM laptop and we mark the computation times in Table V. Decorrelation step massively decreases the computational complexity. SS-TV-decorr performs within 10 (Geneva, Urban) to 67 (Pavia) minutes whereas SS-TV for a dense sampling scheme requires between 11 to 33 hours of computations! This huge gap is due to many costly subiterations of \mathcal{B}_2 projector for dense sampling (see Section V-B), whereas decorrelating method performs it in a single iteration. This gap shrinks by relaxing the projection to allow extra noise (e.g. in Pavia HSI). The classical TVDN method takes about 5 hours (Geneva, Urban), as the corresponding TV minimization runs over a large number of channels (rather than few underlying sources).

To summarize, we show that SS-TV-decorr, meanwhile achieving high robustness against severe undersampling regimes, it can accelerate the recovery process about 30 times compared to the classical TVDN. While finalizing this work we became aware of a recent paper [36] that proposes a source recovery approach similar to (52), albeit for the particular case of uniform sampling and TV regularization. The authors also use a "SVD preprocessing" step for dimensionality reduction and denoising that, contrary to our decorrelation step, does not cancel the effects of the conditioning of the mixing matrix.

TABLE V: Computation times (minutes) of different methods for different sampling schemes and HSIs (subsampling: 1/8, noiseless).

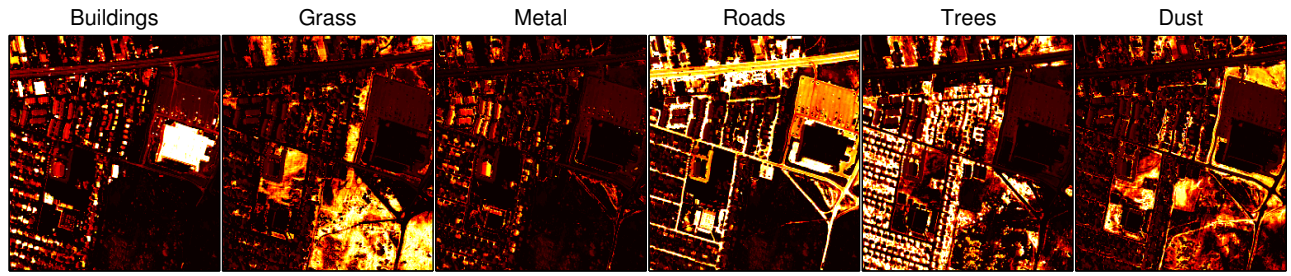
| | SS-IHT | SS-11 | SS-TV | BPDN | TVDN |
|------------------|--------|--------|--------|-------|--------|
| Geneva (dense) | 8.90 | 1.90e3 | 1.95e3 | 37.80 | 352.27 |
| Geneva (-decorr) | 0.46 | 1.12 | 10.23 | — | — |
| Pavia (dense) | 85.70 | 524.93 | 678.12 | — | — |
| Pavia (-decorr) | 3.90 | 7.60 | 66.58 | — | — |
| Urban (dense) | — | 1.47e3 | 1.49e3 | 32.96 | 291.62 |
| Urban (-decorr) | — | 1.16 | 10.01 | — | — |

VII. CONCLUSION

In this paper, we exploited a linear mixture of sources model into a Compressed Sensing (CS) scheme for multichannel signal acquisition and source separation with a particular focus on hyperspectral images. We study three different acquisition schemes (dense, uniform and decorrelated) theoretically and experimentally, and showed that the decorrelating scheme enhances drastically the recovery of the spectral data and its sources. Indeed, our theoretical analysis indicates that, using this scheme, and contrary to the traditional CS approach, the number of measurements does not scale with the number of channels and does not depend on the conditioning of the mixing matrix, as long as the mixed spectra are linearly independent. We conducted several experiments on HSI and showed that we can reconstruct both the HSI and its sources with far fewer measurements and less computational effort than traditional CS approaches. Finally, we showed that it is possible to accurately recover the sources directly from the compressed measurements, avoiding to run a source separation algorithm on the high-dimensional raw data.

REFERENCES

- [1] M. T. Eismann, "Hyperspectral remote sensing." SPIE, 2012.
- [2] C.-I. Chang, *Hyperspectral data exploitation: theory and applications*. Wiley-Interscience, 2007.
- [3] D. L. Donoho, "Compressed sensing," *Information Theory, IEEE Transactions on*, vol. 52, no. 4, pp. 1289–1306, 2006.
- [4] E. J. Candès, J. K. Romberg, and T. Tao, "Stable signal recovery from incomplete and inaccurate measurements," *Communications on pure and applied mathematics*, vol. 59, no. 8, pp. 1207–1223, 2006.
- [5] M. Elad, *Sparse and redundant representations: from theory to applications in signal and image processing*. Springer, 2010.
- [6] J. Wright, Y. Ma, J. Mairal, G. Sapiro, T. Huang, and S. Yan, "Sparse representation for computer vision and pattern recognition," *Proceedings of the IEEE*, vol. 98, no. 6, pp. 1031–1044, June 2010.
- [7] M. F. Duarte and R. G. Baraniuk, "Kronecker compressive sensing," *Image Processing, IEEE Transactions on*, vol. 21, no. 2, pp. 494–504, 2012.
- [8] T. Sun and K. Kelly, "Compressive sensing hyperspectral imager," *Comp. Optical Sensing and Imaging (COSI), San Jose, CA, Oct. 2009*.
- [9] A. Wagadarikar, R. John, R. Willett, and D. Brady, "Single disperser design for coded aperture snapshot spectral imaging," *Applied Optics*, vol. 47, pp. B44–B51, 2008.
- [10] N. Keshava and J. Mustard, "Spectral unmixing," *Signal Processing Magazine, IEEE*, vol. 19, no. 1, pp. 44–57, 2002.
- [11] J. Nascimento and J. Dias, "Vertex component analysis: A fast algorithm to unmix hyperspectral data," *Geoscience and Remote Sensing, IEEE Transactions on*, vol. 43, no. 4, pp. 898–910, 2005.
- [12] J. Wang and C.-I. Chang, "Applications of independent component analysis in endmember extraction and abundance quantification for hyperspectral imagery," *Geoscience and Remote Sensing, IEEE Transactions on*, vol. 44, no. 9, Sept. 2006.
- [13] H. Ren and C.-I. Chang, "Automatic spectral target recognition in hyperspectral imagery," *Aerospace and Electronic Systems, IEEE Transactions on*, vol. 39, no. 4, pp. 1232–1249, Oct. 2003.
- [14] S. Arberet, "Hyper-demix: Blind source separation of hyperspectral images using local ml estimates," in *Proceedings of the 17th International Conference on Image Processing (ICIP 2010)*. Citeseer, 2010.
- [15] M. Golbabaee, S. Arberet, and P. Vanderghenst, "Multichannel compressed sensing via source separation for hyperspectral images," in *Eusipco*, 2010.
- [16] —, "Distributed compressed sensing of hyperspectral images via blind source separation," in *Signals, Systems and Computers (ASILOMAR), The Forty Fourth Asilomar Conference on*. IEEE, 2010.
- [17] L. Rudin, S. Osher, and E. Fatemi, "Nonlinear total variation based noise removal algorithms," *Physica D: Nonlinear Phenomena*, vol. 60, pp. 259–268, 1992.
- [18] R. Tibshirani, "Regression shrinkage and selection via the lasso," *Journal of the Royal Statistical Society. Series B (Methodological)*, pp. 267–288, 1996.
- [19] S. S. Chen, D. L. Donoho, and M. A. Saunders, "Atomic decomposition by basis pursuit," *SIAM journal on scientific computing*, vol. 20, no. 1, pp. 33–61, 1998.
- [20] T. Blumensath and M. Davies, "Iterative thresholding for sparse approximations," *Journal of Fourier Analysis and Applications*, vol. 14, pp. 629–654, 2008.
- [21] B. K. Natarajan, "Sparse approximate solutions to linear systems," *SIAM Journal on Computing*, vol. 24, no. 2, p. 227, 1995.
- [22] S. Mallat and Z. Zhang, "Matching pursuits with time-frequency dictionaries," *Signal Processing, IEEE Transactions on*, vol. 41, no. 12, pp. 3397–3415, 1993.
- [23] E. Candès, "The restricted isometry property and its implications for compressed sensing," *Comptes Rendus Mathématique*, vol. 346, no. 9–10, pp. 589–592, 2008.
- [24] R. Baraniuk, M. Davenport, R. DeVore, and M. Wakin, "A simple proof of the restricted isometry property for random matrices," *Constructive Approximation*, vol. 28, pp. 253–263, 2008.
- [25] R. Penrose, "A generalized inverse for matrices," in *Proc. Cambridge Philos. Soc.*, vol. 51, no. 3. Cambridge Univ Press, 1955, pp. 406–413.
- [26] H. Rauhut, K. Schnass, and P. Vanderghenst, "Compressed sensing and redundant dictionaries," *Information Theory, IEEE Transactions on*, vol. 54, no. 5, pp. 2210–2219, May 2008.
- [27] E. J. Candès, Y. C. Eldar, D. Needell, and P. Randall, "Compressed sensing with coherent and redundant dictionaries," *Applied and Computational Harmonic Analysis*, vol. 31, no. 1, pp. 59–73, 2011.
- [28] P. L. Combettes and J. C. Pesquet, "Proximal splitting methods in signal processing," in: *Fixed-Point Algorithms for Inverse Problems in Science and Engineering*, Springer-Verlag, vol. 49, pp. 185–212, 2011.
- [29] S. Boyd, N. Parikh, E. Chu, B. Peleato, and J. Eckstein, "Distributed optimization and statistical learning via the alternating direction method of multipliers," *Foundations and Trends® in Machine Learning*, vol. 3, no. 1, pp. 1–122, 2011.
- [30] A. Chambolle, "An algorithm for total variation minimization and applications," *Journal of Mathematical Imaging and Vision*, vol. 20, pp. 89–97, 2004.
- [31] J. Duchi, S. Shalev-Shwartz, Y. Singer, and T. Chandra, "Efficient projections onto the l_1 -ball for learning in high dimensions," in *Proceedings of the 25th international conference on Machine learning*, ser. ICML '08, 2008, pp. 272–279.
- [32] M. Fadili and J. Starck, "Monotone operator splitting for optimization problems in sparse recovery," in *Image Processing (ICIP), 2009 16th IEEE International Conference on*. IEEE, 2009, pp. 1461–1464.
- [33] J. Douglas and H. Rachford, "On the numerical solution of heat conduction problems in two and three space variables," *Transactions of the American mathematical Society*, vol. 82, no. 2, pp. 421–439, 1956.
- [34] J. Romberg, "Compressive sensing by random convolution," *SIAM J. Imaging Sciences*, 2009.
- [35] G. Licciardi, F. Pacifici, D. Tuia, S. Prasad, T. West, F. Giacco, C. Thiel, J. Inglada, E. Christophe, J. Chanussot, and P. Gamba, "Decision fusion for the classification of hyperspectral data: Outcome of the 2008 GRS-S data fusion contest," *Geoscience and Remote Sensing, IEEE Transactions on*, vol. 47, no. 11, pp. 3857–3865, 2009.
- [36] C. Li, T. Sun, K. Kelly, and Y. Zhang, "A compressive sensing and unmixing scheme for hyperspectral data processing," *Image Processing, IEEE Transactions on*, vol. 21, no. 3, pp. 1200–1210, March 2012.



(a) Reference: Sources estimated with a BSS algorithm.

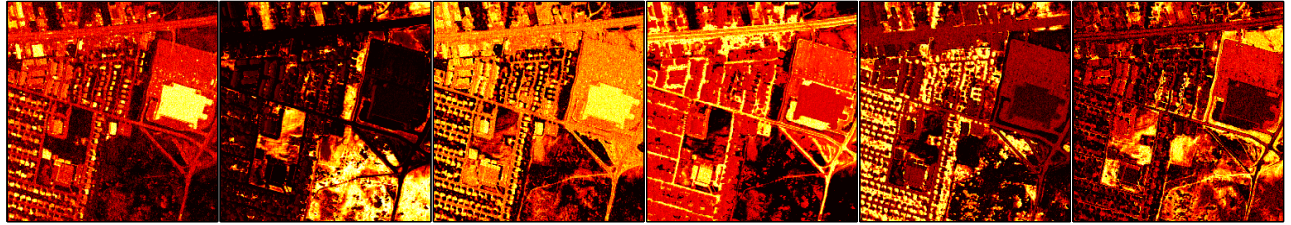
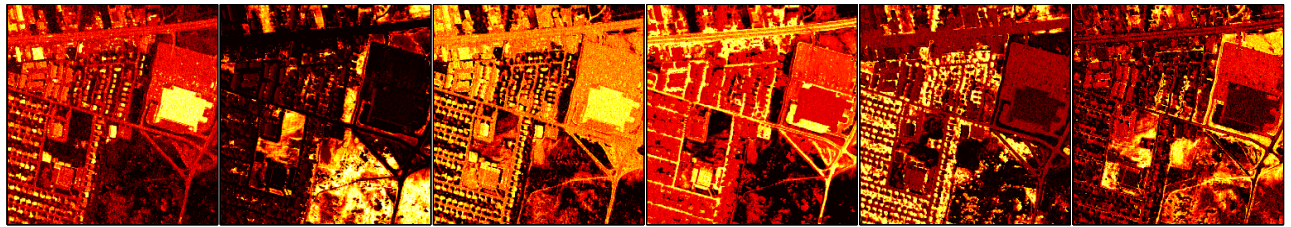
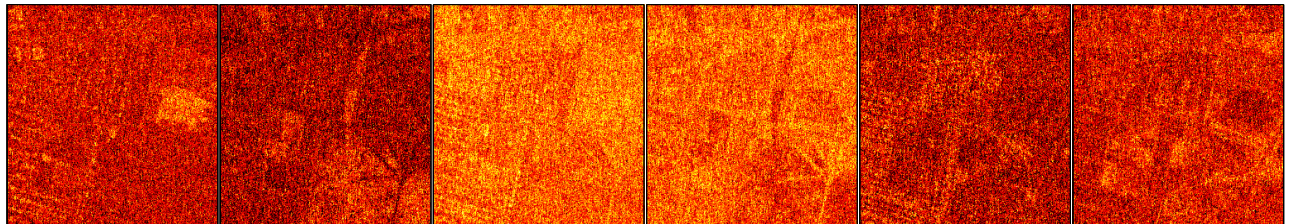
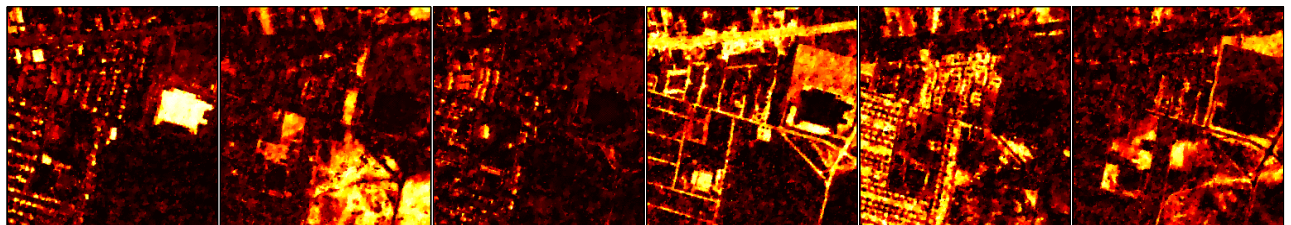
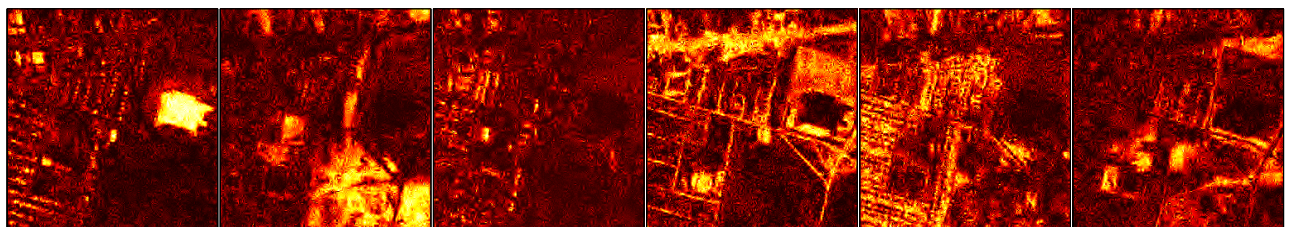
(b) SS-TV (*dense sampling*), source reconstruction SNR: 6.34 dB(c) SS-11 (*dense sampling*), source reconstruction SNR: 6.29 dB(d) SS-TV (*uniform non-decorrelating sampling*), source reconstruction SNR: 1.88 dB(e) SS-TV-decorr (*uniform decorrelating sampling*), source reconstruction SNR: 8.64 dB(f) SS-11-decorr (*uniform decorrelating sampling*), source reconstruction SNR: 5.65 dB

Fig. 3: Estimated source images of Urban HSI using different recovery methods (*i.e.*, TV or wavelet ℓ_1 minimization), and for different sampling mechanisms (subsampling ratio: 1/8, noiseless sampling).